Swelling Effect on Yielding, Elasticity and Fracture of Double-Network Hydrogels with Inhomogeneous First Network

*Yong Zheng[1], Tasuku Nakajima[1,2], Wei Cui[2,3], Chung-Yuen Hui[4,5] and Jian Ping Gong[1,2,4]**

[1]Institute for Chemical Reaction Design and Discovery (WPI-ICReDD), Hokkaido University, Sapporo 001-0021, Japan

[2]Faculty of Advanced Life Science, Hokkaido University, Sapporo 001-0021, Japan

[3]College of Polymer Science and Engineering, State Key Laboratory of Polymer Materials Engineering, Sichuan University, Chengdu, 610065 China

[4]Global Station for Soft Matter, GI-CoRE, Hokkaido University, Sapporo 001-0021, Japan

[5]Field of Theoretical and Applied Mechanics, Sibley School of Mechanical and Aerospace Engineering, Cornell University, Ithaca, NY 14853, USA

*Corresponding author: gong@sci.hokudai.ac.jp

For Table of Contents use only

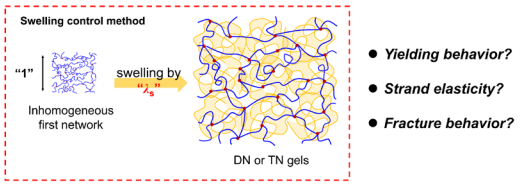

ABSTRACT

Typical double network (DN) gels are formed by free radical polymerization and the constituent network strands have a wide molecular weight distribution. It is important to clarify what determines the specific mechanical behaviors of DN gels with a strongly inhomogeneous first network, including the criteria for the occurrence of yielding and strain hardening during tensile deformation, as well as their impact on the fracture toughness. Herein, we first studied the influence of swelling ratio λ_s of the first network synthesized from radical polymerization on the yielding and strain-hardening of DN and triple-network (TN) gels by tensile tests. We observed scaling relations for the yielding stretch ratio $\lambda_y \propto {\lambda_s}^{-1}$ and engineering yielding stress $\sigma_y \propto {\lambda_s}^{-2}$, like those found for DN hydrogels with a homogeneous first network structure. Furthermore, we found a universal relationship $\lambda_y \sigma_y \propto {\lambda_s}^{-3}$ that is independent of the crosslinking structure of the first network. We found that these scaling relations well agree with the theoretical predictions derived from a simple one-dimensional affine model for fracture of homogeneous network, suggesting the affine swelling effect on fracture of network strands. Next, we showed that the swelling induces much enhanced tension in the inhomogeneous network than in the homogenous network, suggesting non-affine

swelling behavior at network strand scale for the inhomogeneous network. We discussed the molecular origin for the discrepancy between the affine swelling effect on fracture of network strands and non-affine swelling behavior for strand tension. Finally, we investigated the influence of swelling ratio λ_s on the local yielding behavior ahead of the crack tip and the fracture toughness of the DN and TN hydrogels using pure shear tests. We found that crack-tip yielding zone size $h_y \propto {\lambda_s}^1$ and fracture energy $\Gamma \propto {\lambda_s}^{-2}$. Furthermore, we found that $\frac{\Gamma}{h_y} \propto {\lambda_s}^{-3}$ is also independent of crosslinking structure and obeys a universal relationship with the true yielding stress $\lambda_y \sigma_y \propto {\lambda_s}^{-3}$ determined from the tensile tests, which is in excellent agreement with non-linear elastic fracture mechanics theory. This work gives important insights into the specific mechanical behaviors of the DN gels with inhomogeneous first network.

INTRODUCTION

Mechanically robust soft materials have attracted great attention not only in traditional engineering but also in emerging material fields such as soft wearable electronic devices[1] , soft robotics[2], and biomedical materials[3, 4]. Various strategies to fabricate mechanically robust soft materials especially tough gels have been developed during the past decades.[5-12] Among these efforts, the double-network (DN) concept provides an effective and general strategy that can be applied to various polymer combinations to fabricate strong and tough gels and elastomers.[7, 9, 12-16] Specifically, DN hydrogels with optimized structure exhibit superior mechanical properties such as enhanced fracture energies between 10^3–10^4 J m^{-2} compared to the conventional weak gels with fracture energies between 10^0–10^2 J m^{-2}.[9]

Tough DN gels or elastomers are interpenetrating network materials, consisting of two contrasting networks, *i.e.*, one network is brittle and sparse and the other is stretchable and dense.[9, 17] During the deformation process, a large number of the first brittle network strands sacrificially rupture and dissipate a large amount of energy before the fracture of the stretchable second network, which leads to the extremely high toughness of a DN material.[18-20] Such sacrificial fracture of the first network occurs in a wide spatial region and leads to unique mechanical behaviors, including a yielding-like phenomenon and strain-hardening before global fracture of the material, accompanied by an irreversible mechanical hysteresis during the tensile test.[18, 19, 21] Many efforts have been made to elucidate the molecular mechanisms of the mechanical behaviors and internal damage in DN hydrogels. The yielding of DN hydrogels has been related to the global internal fracture of first network perpendicular to the tensile direction, while at further increased deformation in the strain-hardening regime, internal fracture in the tensile direction becomes dominant.[21,22]

For DN hydrogels with a well-controlled, relatively homogeneous tetra-PEG first network, the effect of pre-swelling ratio λ_s of the first network on yielding has been studied and it has been found that the yielding stretch ratio $\lambda_y \propto {\lambda_s}^{-1}$ and the engineering yielding stress $\sigma_y \propto {\lambda_s}^{-2}$.[21] These results suggest that (1) the homogenous network swells affinely; (2) the yielding stretch ratio is proportional to the stretching limit while the engineering yielding stress is proportional to the area density of the first network strands.[21]

On the other hand, conventional DN gels and multi-network materials have high

structural inhomogeneity down to nanoscale[23-33], and the polymer strands have a wide molecular weight distribution. For example, a recent study by direct TEM observation has shown that the polymer networks synthesized by free radical copolymerization of monomers and cross-linkers have a strong network heterogeneity.[23] Previous studies have shown that swelling increases the inhomogeneity of a polymer network.[33-35] These observations suggest that the swelling of heterogeneous networks is non-affine at polymer strand level. Thereby, intuitively, one expects that the yielding of DN gels from a heterogeneous first network will show quite different scaling dependence on the pre-swelling ratio λ_s with that of DN gels from a homogeneous network.

Our goal here is to study the swelling effect on the mechanical behaviors, thereby elucidating the molecular mechanism of yielding, strain-hardening, and fracture of DN hydrogels with an inhomogeneous first network synthesized from free radical copolymerization. The paper is organized as follows. First, we performed tensile tests on three sets of DN and TN gels to clarify how yielding and strain-hardening depend on the pre-swelling ratio λ_s of the first network. Then we derived fracture stress and strain and their dependence on λ_s for a homogeneous network based on a one-dimensional (1-D) affine model. We discussed the correlations between the observed yielding stretch ratio /stress and the fracture stretch ratio/stress predicted from the model. Further, we studied the effect of swelling ratio λ_s on network elasticity of inhomogeneous first-network. Finally, we performed pure shear fracture tests to investigate how λ_s influences the local yielding ahead of crack tip and thus the fracture toughness of DN gels. We discussed quantitatively the universal relation between the

true yielding stress from the tensile tests and the crack-tip yielding zone size and fracture energy from the pure shear tests, and compare the results with the nonlinear elastic fracture mechanics theory.

RESULTS AND DISCUSSION

Methods to tune the swelling of the first network.

We adopt DN hydrogels comprising poly(2-acrylamido-2-methylpropane sulfonic acid sodium salt) (PNaAMPS) as the first network and polyacrylamide (PAAm) as the second network, both networks are crosslinked by *N*,*N*′-methylenebis(acrylamide) (MBAA). The DN gels were synthesized in water via a two-step sequential free radical polymerization process.[36] The TN gels were obtained by a third step synthesis of PAAm network in DN gels.[37] After synthesis of DN and TN gels, we systematically tuned the pre-stretching state of the first network by swelling/deswelling of the gels using two post-synthesis methods. The first of these is the osmotic pressure method, where DN and TN gels were immersed in PEG solution of a prescribed concentration, which exerted osmotic pressure and resulted in gel deswelling.[38] For the second molecular stent method, the DN and TN gels were immersed in AMPS monomer solution and then the polymerization of AMPS was performed to form linear polyelectrolytes in the gels, which increased internal osmotic pressure of the gels and resulted in gel swelling in pure water.[13] Since the first network has a much higher chemical crosslinking density than the second network, the changes in the swelling after synthesis brings significant effect on the pre-stretching state of the first network but not of the second network. We denoted the as-prepared first network gel as state 0, the as-prepared DN and TN as state

1 and 2, respectively, and the swollen/deswollen DN and TN gels as state 3. The detailed process is illustrated in Figure 1. The linear swelling ratios of first network in each state in relative to its previous state are denoted as $\lambda_{s,n}$(n=1,2,3). Specifically, $\lambda_{s,1}$ denotes the swelling ratio of first network in the as-prepared DN gels (state 1) relative to its as-prepared state (state 0), $\lambda_{s,2}$ denotes the swelling ratio of as-prepared TN to as-prepared DN, and $\lambda_{s,3}$ denotes swelling ratio of TN or DN after post swelling/deswelling treatment to their as-prepared state. Thus, the overall swelling ratio of first network relative to its as-prepared state is $\lambda_s=\lambda_{s,1}\lambda_{s,2}\lambda_{s,3}$, where $\lambda_{s,2}$=1 for DN gels subjected to post-swelling/deswelling treatment. The first single network is denoted as SN-*x*, and the DN and TN gels are denoted as DN-*x*-λ_s and TN-*x*-λ_s gels for simplicity, where *x* represents the crosslinking density of the first network. The sample codes, formulation in synthesis, and swelling ratios at different state of the synthesized DN and TN gels were listed in Tables S1 and S2. Three sets of gels with various λ_s, DN-3-λ_s, DN-4.5-λ_s and TN-4.5-λ_s, were prepared in addition to two other types of virgin DN gels with different first network crosslinking density (DN-4-2.23, DN-6-1.82). It should be mentioned that, to obtain ductile DN and TN gels with distinct yielding and strain-hardening features, the monomer concentrations for second network (C_{2nd}) and third network (C_{3rd}) in DN-4.5-λ_s and TN-4.5-λ_s are 3.0 M while the monomer concentration (C_{2nd}) is 2.0 M for second network in DN-3-λ_s. With these gels, we intend to discuss the effect of λ_s with different crosslinker density (*x*) of first network and relative concentration of PAAm network to the first network.

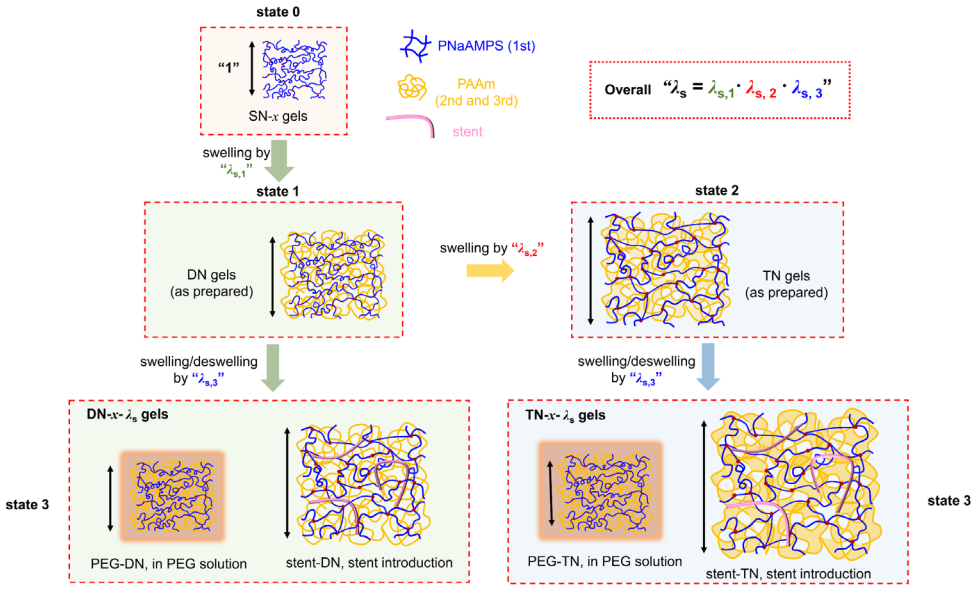

Figure 1. Schematic illustration of varying the swelling ratios, λ_s of the first network (blue) in DN or TN gels by various methods. The as-prepared first network gel, the as prepared DN and TN gels are denoted as state 0, 1 and 2, respectively, and the swollen/deswollen DN and TN gels are denoted as state 3. $\lambda_{s,1}$ denotes the swelling ratio of first network in the as prepared DN gels (state 1) in relative to its as prepared state (state 0), $\lambda_{s,2}$ denotes the swelling ratio of as-prepared TN to as-prepared DN, and $\lambda_{s,3}$ denotes swelling ratio of post swelling treated DN or TN relative to their as-prepared states. Thus, the overall swelling ratio of first network relative to its as-prepared state (state 0) $\lambda_s = \lambda_{s,1}\,\lambda_{s,2}\,\lambda_{s,3}$, where $\lambda_{s,2}$=1 for post swelling/deswelling DN gels. The single first network is denoted as SN-x, DN and TN gels are denoted as DN-x-λ_s and TN-x-λ_s, where x represents the in feed crosslinker density of the first network. The detailed information of samples is listed in Tables S1 and S2.

Uniaxial tensile behaviors.

Uniaxial tensile tests were performed to quantify the yielding tensile behaviors. Figures 2(A, i)−2(C, i) show the tensile stress-stretch ratio curves for three sets of samples, DN-3-λ_s, DN-4.5-λ_s and TN-4.5-λ_s gels. Basically, all samples except the ones with high λ_s exhibit remarkable yielding and necking phenomena. We first quantify the relations between yielding conditions (*i.e.*, yielding stretch ratio λ_y and yielding tensile (nominal) stress σ_y) and swelling ratio λ_s. λ_y and σ_y are plotted as functions of λ_s with logarithmic axes in Figures 2(A, ii, iii)−2(C, ii, iii). Scaling relationships, $\lambda_y \propto {\lambda_s}^{-1}$ and $\sigma_y \propto {\lambda_s}^{-2}$, are observed for *all* three sets of DN and TN gels, which indicates an invariant yielding stretch ratio and engineering yielding stress when these quantities are normalized by the overall swelling ratio of the as-prepared state of the first network. These behaviors are the same with the previous study on the DN hydrogels with a fairly homogeneous tetra-PEG first network.[21] These results suggest that the inhomogeneous first network also swells affinely and the yielding stretching ratio is proportional to the average stretching limit and yielding stress to the areal density of first network strands, like the homogeneous first network.

We further discuss the effect of stretchable PAAm network concentration and crosslinking density of first network on yielding by plotting λ_y and σ_y against λ_s for all sets of DN and TN gels in Figures 3A and 3B. There are two interesting findings: (1) the λ_y and σ_y of DN-4.5-λ_s and TN-4.5-λ_s gels overlap very well. Because they are prepared from the same PNaAMPS (as-prepared) first network, the relative concentration of PAAm network to the PNaAMPS network in the TN is much higher

than in the DN. The well overlapped data of λ_y and σ_y for DN-4.5-λ_s and TN-4.5-λ_s gels indicate that the first network topological structure predominates the yielding criteria and the stretchable PAAm network concentration hardly influence the yielding condition. This is consistent with previous studies.[21, 39] Because the PAAm network concentration hardly affect the yielding condition, we can discuss the effect of crosslinking density of first network on yielding by comparing the DN-3-λ_s and DN-4.5-λ_s samples even though they have different C_{2nd}. We find that: (2) with a lower crosslinking density in first network (see Figures 3A and 3B), λ_y increases while σ_y decreases at the same λ_s. This is reasonable because decreasing the crosslinking density results in increased average strand molecular weight and decreased strand density.

Surprisingly, we observed that for all sets of DN-3-λ_s gels, DN-4.5-λ_s, TN-4.5-λ_s, DN-6-1.82 and DN-4-2.23 gels, the product of $\sigma_y\ \lambda_y$ (which could be understood as the true yielding stress $\sigma_{T,y}$) fall on a single scaling line of $\sigma_y\ \lambda_y \propto {\lambda_s}^{-3}$, as shown in Figure 3C. This result indicates that $\sigma_y\ \lambda_y$ is invariant with crosslinking density of the first network. Note that in all these different sets of gels, the first networks were prepared with the same monomer concentration but with varied crosslinker concentration.

In addition to λ_y and σ_y, the plateau stress after yielding, $\sigma_{plateau}$ and the stretch ratio at the onset of strain-hardening, λ_{hard} are important mechanical properties for DN gels, as they reflect the mechanical interaction between two networks. The question is how $\sigma_{plateau}$ and λ_{hard}, depend on the swelling ratio of first network λ_s=$\lambda_{s,1}\lambda_{s,2}\lambda_{s,3}$ and the swelling ratio of second network $\lambda_{s,2nd}$=$\lambda_{s,2}\lambda_{s,3}$. Figure 4(A, i) and 4(B, i),

summarized and plotted $\sigma_{plateau}$ and λ_{hard} against λ_s respectively. Scaling relationships of $\sigma_{plateau} \propto {\lambda_s}^{-2}$ and $\lambda_{hard} \propto {\lambda_s}^{-1}$are observed. These results suggest that $\sigma_{plateau}$ and λ_{hard} are essentially related to the strand density of the first network. To check how the swelling ratio of second network $\lambda_{s,2nd}$=$\lambda_{s,2}\lambda_{s,3}$ influence $\sigma_{plateau}$ and λ_{hard}, we plot the $\sigma_{plateau}$ and λ_{hard} against $\lambda_{s,2nd}$ in Figure 4(A, ii) and 4(B, ii), respectively. By comparing the $\sigma_{plateau}$ and λ_{hard} of DN-4.5-λ_s and TN-4.5-λ_s gels, we observe that the TN-4.5-λ_s gels show much reduced λ_{hard} but almost the same $\sigma_{plateau}$ compared to that of DN-4.5-λ_s gels at the same $\lambda_{s,2nd}$. This result clearly shows that increasing the stretchable PAAm network concentration has a strong effect on the strain-hardening phenomenon but only has a negligible effect on the plateau stress after yielding. On the other hand, C_{2nd} is a little higher in DN-4.5-λ_s gels (C_{2nd} = 3.0 M) than in DN-3-λ_s gels (C_{2nd} = 2.0 M). The comparison between DN-3-λ_s and DN-4.5- λ_s gels also supports the finding that increasing the PAAm network concentration reduces λ_{hard}. This is reasonable because the strain-hardening of DN should strongly rely on the strain-hardening of PAAm itself, and increasing the PAAm network concentration will increase the entanglement density of PAAm network to first network and between the PAAm network, thus affecting the load-transfer between two networks and causing strain-hardening occur at relatively small stretching.[40]

We next rescale the tensile stress σ and stretch ratio λ for DN-3-λ_s, DN-4.5-λ_s and TN-4.5-λ_s gels by multiplying σ by ${\lambda_s}^2$ and λ by λ_s; that is, we normalized the stress and the stretch ratio by the strand density and stretch ratio relative to the as prepared first network state.[15] As shown in Figure S1, for all series of DN and TN gels, the

rescaled stress ($\sigma\lambda_s^2$) versus stretch ratio ($\lambda\lambda_s$) curves almost overlap with each other even beyond the yielding point for small λ_s (< 3.3) but deviate slightly at rather large λ_s. The well-overlapped curves for small λ_s are reasonable because the relative concentration of two network is kept constant for the same set of samples. The slight deviation at rather large λ_s suggests that a small number of strands in the first network have already been damaged by swelling-induced overstretching.

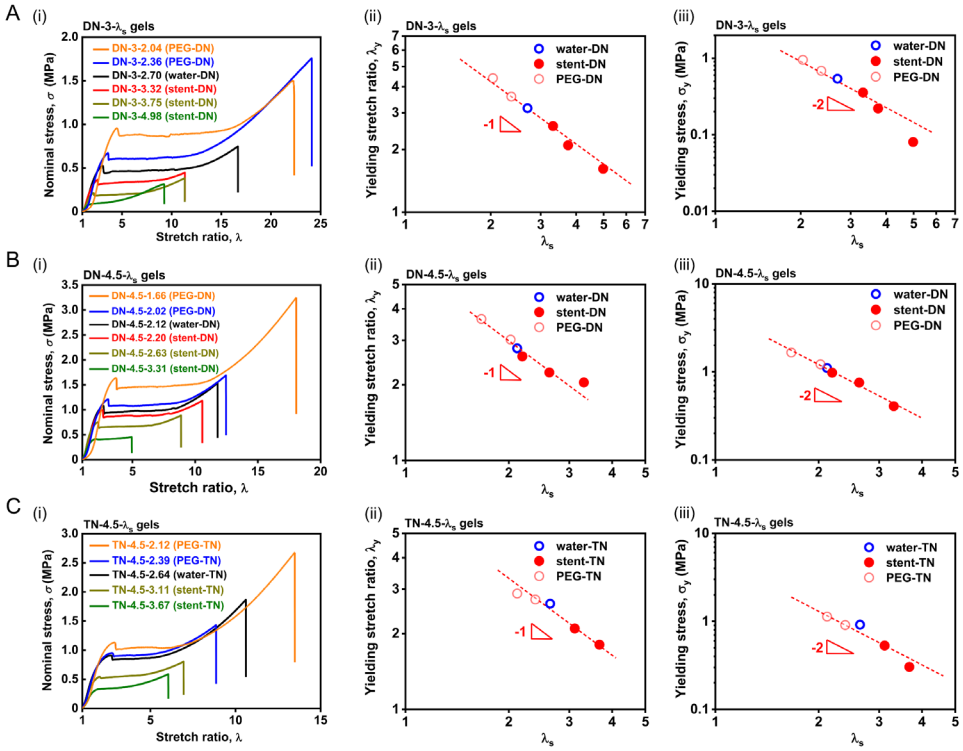

Figure 2. Uniaxial tensile behaviors of various series of DN and TN gels. (A-C) Stress σ-stretch ratio λ curves (i), yielding stretch ratio λ_y dependence on λ_s (ii) and yielding stress σ_y dependence on λ_s (iii) for (A) DN-3-λ_s gels, (B) DN-4.5-λ_s gels and (C) TN-4.5-λ_s gels.

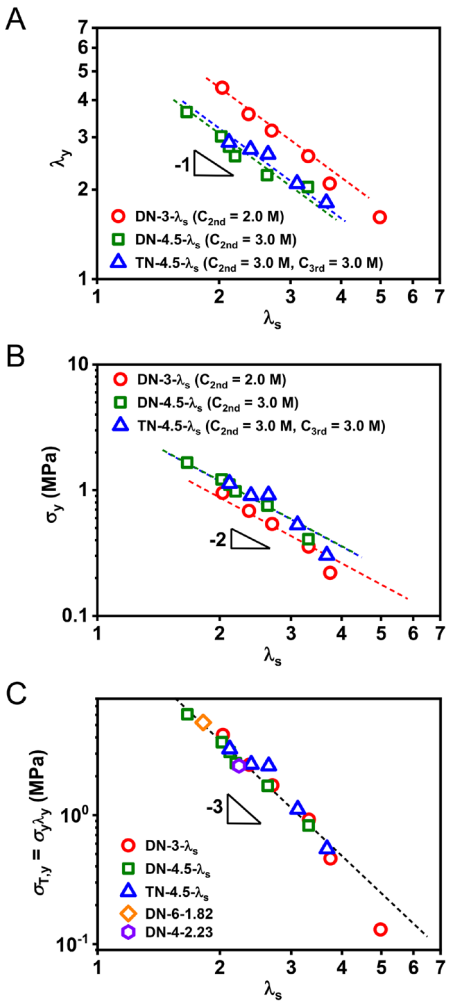

Figure 3. Effect of swelling ratio of first network $\lambda_s = \lambda_{s,1}\lambda_{s,2}\lambda_{s,3}$ on the yielding behaviors in various series of DN and TN gels. (A, B) Yielding stress σ_y (A) and yielding stretch ratio λ_y (B) dependences on λ_s. (C) The true yielding stress $\sigma_{T,y} = \sigma_y \lambda_y$ as a function of λ_s for various series of DN and TN gels.

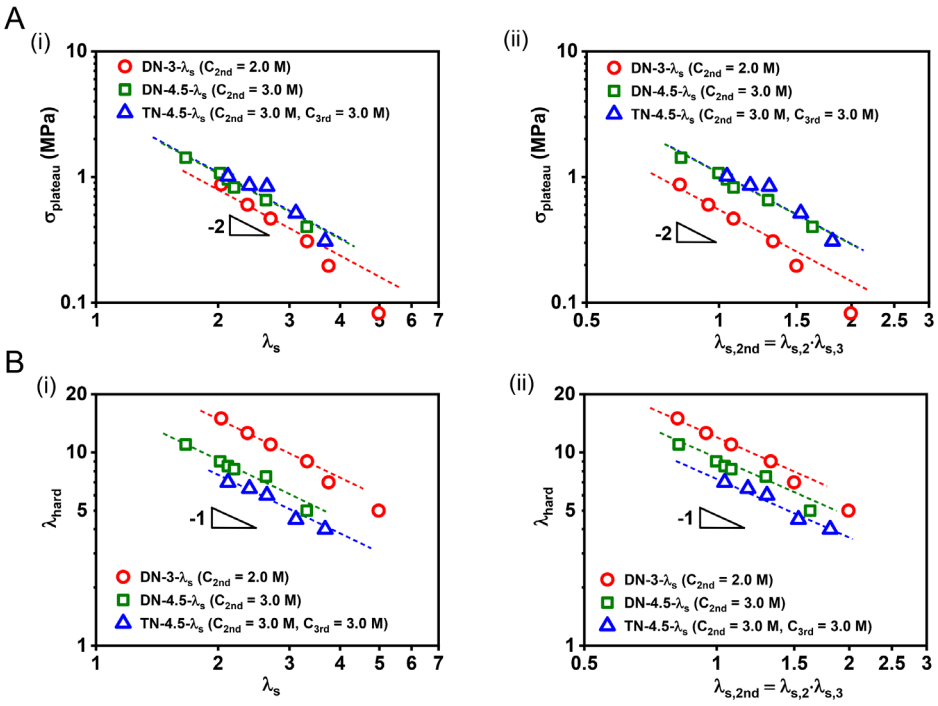

Figure 4. Effect of swelling ratio of first network $\lambda_s = \lambda_{s,1}\lambda_{s,2}\lambda_{s,3}$ and swelling ratio of second network $\lambda_{s,2nd} = \lambda_{s,2}\lambda_{s,3}$ on the tensile behaviors in various series of DN and TN gels. (A) Plateau stress $\sigma_{plateau}$ dependence on λ_s (i) and $\lambda_{s,2}\lambda_{s,3}$ (ii). (B) Strain-hardening stretch ratio λ_{hard} dependence on λ_s (i) and $\lambda_{s,2}\lambda_{s,3}$ (ii).

A 1-D affine model for fracture of homogeneous network to discuss the molecular origin of yielding.

To discuss the molecular mechanism of the observed yielding behavior, here we derive the maximum possible stretching ratio λ_{max} and breaking stress σ_{max} of a homogeneous network with Kuhn monomer number N_x per strand. The network swells with a linear swelling ratio λ_s in relative to its as-prepared state. Here, we only consider the polymer strands aligning in the tensile direction (1-D). Assuming the affine deformation, the macro stretch ratio of a network and the strand deformation ratio along the stretch direction are the same,

$$\lambda_{max} = \frac{R_{max}}{R} \quad (1)$$

where R_{max} represents the maximum length of a strand in its stretching limit, R represents its end-to-end distance before stretching. The maximum nominal stress is

$$\sigma_{max} = f_b v_e R \quad (2)$$

where f_b is the force to break a single first network strand, v_e is the number density of the first network strands per volume, and $v_e R$ is the number density of the first network strands per area.[41] For affine swelling,

$$R = \lambda_s R_0 \quad (3)$$

$$v_e = \frac{v_{e,0}}{{\lambda_s}^3} \quad (4)$$

Here R_0 represents the end-to-end distance of a network strand and $v_{e,0}$ is the number of the first network strands per volume of the as-prepared network. To relate R_{max} and R_0 with N_x, here we simply assume that R_0 equals to that of a polymer chain of the same N_x in dilute solution, then $R_0 = b{N_x}^{\nu}$, where ν is Flory exponent and b is the Kuhn length.[16, 42] Using $R_{max} = bN_x$, we have

$$\lambda_{max} = \frac{R_{max}}{\lambda_s R_0} = {N_x}^{1-\nu}/\lambda_s \quad (5)$$

$$\sigma_{max} = f_b v_{e,0} R_0/{\lambda_s}^2 = f_b b v_{e,0} {N_x}^{\nu}/{\lambda_s}^2 \quad (6)$$

$$\sigma_{max}\lambda_{max} = f_b b v_{e,0} N_x/{\lambda_s}^3 \quad (7)$$

On the other hand, $N_x = \frac{C_0}{v_{e,0}}$, where C_0 is the total Kuhn monomer number per volume of the elastically effective strands. So,

$$\lambda_{max} = \left(\frac{C_0}{v_{e,0}}\right)^{1-\nu}/\lambda_s \quad (8)$$

$$\sigma_{max} = f_b b {v_{e,0}}^{1-\nu} {C_0}^{\nu}/{\lambda_s}^2 \quad (9)$$

$$\sigma_{max}\lambda_{max} = f_b b C_0/{\lambda_s}^3 \qquad (10)$$

It is interesting to note that the true maximum stress $\sigma_{max,}\lambda_{max}$ is independent of the network structure $v_{e,0}$ and is proportional to the Kuhn monomer concentration C_0 of the network, as shown by Eqn. (10).

Here, we compare the scaling relations predicted for fracture of an ideally homogeneous network (Eqn. (8-10)) and the observed yielding behaviors of DN gels. We see that despite the network inhomogeneity, the experimentally observed yielding stretch ratio $\lambda_y \propto {\lambda_s}^{-1}$ and yielding stress $\sigma_y \propto {\lambda_s}^{-2}$ have the same dependences on the swelling ratio λ_s as those of λ_{max} and σ_{max} derived from the 1-D affine model for fracture of a homogeneous model. Furthermore, our experimental observation showing that $\sigma_y \lambda_y \propto {\lambda_s}^{-3}$ is independent of crosslinking density in first network, and this is also in good agreement with the results that $\sigma_{max}\lambda_{max}$ is independent of $v_{e,0}$ but linearly depends on C_0 (Eqn. (10)). These excellent agreements of the scaling relations suggest that the swelling effect on the yielding of DN gels with inhomogeneous first networks could be simply described by a fracture model for a homogenous network. This result is surprising since previous observations suggest non-affine swelling of inhomogeneous networks. [33-35] In the next section, we further discuss this interesting phenomenon from the effect of swelling on the elasticity of the network.

Effect of network inhomogeneity on the strand elasticity of first network

Since strands close to their stretching limit will bear more tension against swelling, we can discuss the network inhomogeneity from the relationship between elastic modulus and pre-swelling ratio λ_s. [34]

The Young's modulus, E, of a polymer network is related to the number density of the elastically effective strands, v_e, and the elastic free energy per strand, F_{el}, as [43]

$$E \sim v_e F_{el} \sim v_{e,0} {\lambda_s}^{-3} F_{el}. \quad (11)$$

Here we assume that the strands in the as-prepared network (λ_s=1) are in unperturbed Gaussian state, $F_{el}^0 = k_B T$ and the Young's modulus of the as-prepared network $E_0 \sim v_{e,0} k_B T$.[43] We have

$$\frac{F_{el}}{k_B T} = \frac{E}{E_0} {\lambda_s}^3. \quad (12)$$

Since F_{el} linearly increases with the Kuhn number N_x of a strand, here we discuss the elastic energy per Kuhn segment of a strand,

$$\frac{F_{el}}{N_x k_B T} = \frac{E}{N_x E_0} {\lambda_s}^3 = \frac{2E{\lambda_s}^3}{3k_B T C_0}. \quad (13)$$

In the right equation, we assume phantom network model ($E_0 = \frac{3}{2} v_{e,0} k_B T$). On the other hand, F_{el} is a function of the end-to-end distance of a strand relative to its stretching limit, $\frac{R}{R_{max}}$.[16, 21] For example, the freely-jointed chain (FJC) model describes the elastic free energy of a strand F_{el} [14, 43, 44]

$$\frac{F_{el}}{k_B T} = N_x \left[\frac{\left(\frac{R}{R_{max}}\right)^2}{2} - \ln\left(1 - \left(\frac{R}{R_{max}}\right)^2\right) \right] \quad (14)$$

As the strands are stretched by swelling, F_{el} increases with λ_s, especially when the strands are stretched close to their stretching limit. In the 1-D affine model, $\frac{R}{R_{max}} = \frac{\lambda_s}{\lambda_{max,0}}$, where $\lambda_{max,0} = \frac{R_{max}}{R_0}$. $\lambda_{max,0}$ represents the theoretical stretching limit of first network strands in relative to their as prepared reference state. Thus, a plot of $\frac{F_{el}^0}{N_x k_B T} = \frac{E}{N_x E_0} {\lambda_s}^3 = \frac{2E{\lambda_s}^3}{3k_B T C_0}$ against $\frac{\lambda_s}{\lambda_{max,0}}$ reveals the effect of swelling on the elastic energy per Kuhn segment of the first network strands. Although Eqn. (13) is derived for an ideal homogeneous rubbery network, this equation allows us to reveal some important

features of the inhomogeneous networks. For a heterogeneous network with broad distribution in strands length and density, $\frac{\lambda_s}{\lambda_{max,0}}$ corresponds to the average.

Figure 5A plots the Young's modulus E (Table S3) as a function of λ_s for various DN-3-λ_s gels, DN-4.5-λ_s and TN-4.5-λ_s gels. All three series of DN and TN hydrogels exhibit an initial increase in Young's modulus with λ_s, followed by a gradual decrease for larger values of λ_s. In DN and TN gels, the Young's modulus of DN and TN gels is dominantly from the first network and the contribution from the soft PAAm is negligible. As shown in Figure 5B, all three sets of gel data collapsed on a master curve of $\frac{2E{\lambda_s}^3}{3k_BTC_0} \sim \left(\frac{\lambda_s}{\lambda_{max,0}}\right)^{6.1}$ in the small range of $\frac{\lambda_s}{\lambda_{max,0}}$ between 0.2 and 0.5. This result is important, since it shows that the average elastic energy of the first network strands exhibit a significantly stronger dependence on λ_s than the relation of $F_{el} \sim {\lambda_s}^2$ predicted for Gaussian chains as well as from the freely-jointed chain (FJC) model.[14, 43, 44] This indicates that, due to heterogeneity of the first network, a very strong finite extensibility effect already plays a role in determining the average elastic energy of strands even though the average $\frac{\lambda_s}{\lambda_{max,0}}$ is well below 0.5. In other words, some strands in first network are already very close to their stretching limits although the average strands are not yet.

To further justify this network inhomogeneity effect on swelling, we present the data for DN hydrogels with a relatively homogeneous tetra-PEG first network in Figure 5B for comparison.[21] A much weaker dependence of $\frac{F_{el}}{N_x k_B T} = \frac{E}{N_x E_0}{\lambda_s}^3 \sim \left(\frac{\lambda_s}{\lambda_{max,0}}\right)^{2.7}$ is observed for DN hydrogels with a homogeneous tetra-PEG first network in the $\frac{\lambda_s}{\lambda_{max,0}}$ range of 0.1 ~ 0.5, which is close to the predicted relation of $F_{el} \sim {\lambda_s}^2$ for Gaussian

chains.

Thus, the first network of our DN gels from free radical polymerization is very inhomogeneous, and strong strain-hardening occurs for some strands even at relatively low swelling ratio. This explains why a relatively homogenous tetra-PEG gels exhibited a lower modulus than the PNaAMPS gels when compared at the similar swelling ratio.[21,43] These results on swelling-induced strain-hardening of heterogeneous network indicate that the swelling dependence is non-affine at strand scale, which is consistent with the previous reports that swelling enhances the inhomogeneity of polymer network.[33-35] Then how to understand the discrepancy between this non-affine swelling behavior observed from elastic modulus (at small deformation) and the affine swelling behavior observed from yielding (at fracture) of the first network? We postulate that breaking of strands prior to yielding, as seen by the remarkable strain-softening and mechanical hysteresis before yielding,[20,22,36] homogenizes the first network structure to show affine swelling dependence at yielding.

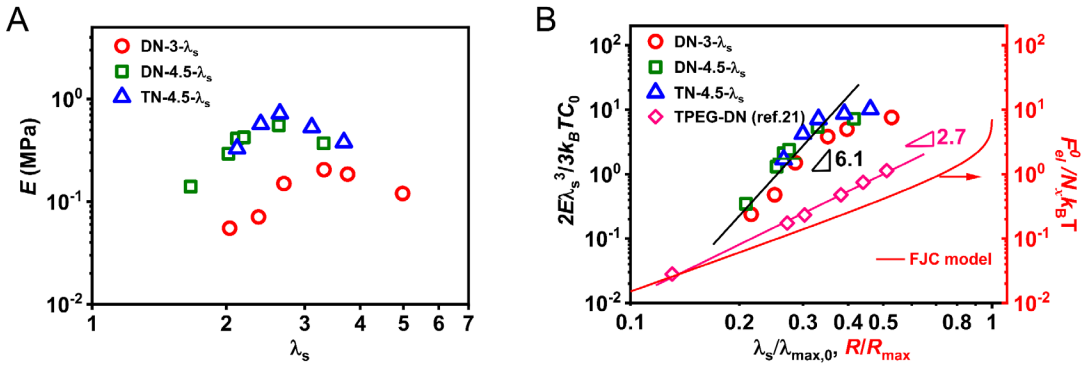

Figure 5. Effect of network inhomogeneity on strand elasticity of the first network. (A) Young's modulus E as a function of pre-swelling ratio of first network λ_s and (B) dependence of elastic energy per Kuhn segment of strands $\frac{F_{el}^0}{N_x k_B T} = \frac{2E{\lambda_s}^3}{3k_B T C_0}$ on $\frac{\lambda_s}{\lambda_{max,0}}$ for

different gels. $\lambda_{max,0}$ represents the theoretical stretching limit of first network strands in relative to their as prepared reference state. In comparison, the data for TPEG-DN hydrogels with homogeneous first network structure (using equation of $\frac{E}{N_x E_0}\lambda_s{}^3$ for calculation of elastic energy per Kuhn segment of strands) and from FJC model are also shown. The results for TPEG-DN hydrogels were calculated based on the results shown in ref [21]. The detailed parameters used for the plots in (B) are shown in SI (Table S4 and supplementary text).

Quantitatively relating yielding and fracture initiation.

Previous studies have shown that local yielding also remarkably occurs at crack tip for DN materials including DN gels and multiple-network elastomers[12, 18, 45-49] (Figure 6B), it is easy to imagine that the local yielding behavior ahead of crack tip should also be controlled by the average stretching limit and strand density of first network. We next study how the pre-swelling ratio of first network strands influences the local yielding zone size and energy dissipation ahead of crack tip and thus the fracture toughness of DN gels.

As reported in a previous work, the yielding zone (necking zone), where local yielding significantly occurs, can be directly observed in front of the crack tip using the birefringence retardation measurement.[45] Here, we investigate the fracture and local yielding behaviors at the onset of crack growth in the pure shear fracture tests by applying the same experimental set-up shown in Figure 6A. The samples were placed between two crossed circular polarized films, and the two films and sample were placed between a white lamp and a video camera.[45] Real-time imaging of the birefringence for the gel samples under pure-shear condition allows us to investigate damage zone size ahead of crack tip at fracture initiation. Figures 6C−E show the birefringence images

around crack tip for three sets of gel samples, DN-3-λ_s, DN-4.5-λ_s and TN-4.5-λ_s gels. The yielding zone area S (mm^2) at the deformed state is directly estimated from the strong birefringence area ahead of crack tips. The characteristic yielding zone size at the undeformed state, h_y (mm), is roughly estimated using the relation of $h_y = S^{0.5}/\lambda_{yz}$ as reported in our previous work, where λ_{yz} is the stretch ratio of the yielding zone in uniaxial tensile test.[45] Here, λ_{yz} is estimated using the stretch ratio at the onset of strain-hardening (λ_{hard}) in uniaxial tensile test, corresponding to the stretch ratio of the yielding zone. We also measure the fracture energy Γ (J/m^2) for all these samples from their unnotched and notched stress-stretch ratio curves under pure-shear conditions.

The fracture energy Γ, yielding zone area S, yielding zone deformation ratio λ_{yz}, yielding zone size h_y, and yielding true stress $\sigma_{T,y}$ for various DN-3-λ_s gels, DN-4.5-λ_s and TN-4.5-λ_s gels are summarized in Table S5. We plot the yielding zone size h_y and fracture energy Γ against swelling ratio λ_s in Figures 7A and 7B. We found that h_y slightly increases with λ_s, following roughly a scaling relation of $h_y \propto \lambda_s$ while fracture energy Γ follows a relation of $\Gamma \propto {\lambda_s}^{-2}$ for various series of DN and TN gels. The relation $\Gamma \propto {\lambda_s}^{-2}$ has also been observed for multiple network elastomers containing sacrificial first network recently by Creton and coworkers.[48] Notably, we also find that the data for DN-4.5-λ_s and TN-4.5-λ_s nicely fall into the same scaling line, which is different from the scaling line for DN-3-λ_s gels (Figure 7B). This is reasonable considering DN-4.5-λ_s and TN-4.5-λ_s gels are prepared from the same PNaAMPS-4.5-1 networks. This result clearly indicates that the strand density of first network in the yielding zone contributes to fracture toughness of DN gels, and the

second network concentration hardly affects the fracture toughness of DN gels as long as the second network can provide a stretchable matrix. We further found that for all sets of DN-3-λ_s gels, DN-4.5-λ_s, TN-4.5-λ_s gels, the ratio Γ/h_y fall on a single scaling line $\Gamma/h_y \propto {\lambda_s}^{-3}$as shown in Figure 7C. This result indicates that Γ/h_y is independent of crosslinking density in the first network, in similar with $\sigma_y\ \lambda_y \propto {\lambda_s}^{-3}$ observed in tensile test.

Next, we quantitatively relate local yielding zone size, fracture energy at crack initiation, and the tensile yielding stress using nonlinear elastic fracture mechanics theory. For crack tip fields in generalized neo-Hookean soft elastic solids subjected to large deformation under Mode I plane stress conditions, uniaxial tension dominates the stress field near the crack tip.[50, 51] The asymptotic near tip stress field analysis gives the form of tension ahead of crack tip: $\sigma_T = \gamma \frac{\Gamma}{r}$, where σ_T is the true stress in tension direction, *r* is the radial coordinate of a material point in the undeformed configuration, and γ is a numerical constant that depends on the angular coordinate and strain hardening characteristics.[45, 50, 51] By setting the asymptotic near tip stress field (true stress, σ_T) to the true critical stress for yielding, $\sigma_{T,y}$, and *r* to the necking zone size h_y, we obtain

$$\sigma_{T,y} = \gamma \frac{\Gamma}{h_y}. \qquad (15)$$

This relation predicts the quantitative coupling between local yielding size, yielding true stress and fracture energy at crack initiation. To confirm if the local true yielding stress at the crack tip equals to that of uniaxial tensile test, here we plot $\frac{\Gamma}{h_y}$ from fracture tests against $\sigma_{T,y} = \sigma_y\ \lambda_y$ from tensile test for the three series of DN-3-λ_s gels, DN-

4.5-λ_s and TN-4.5-λ_s gels (Table S5 and Figure 3C) with a wide range of λ_s. As shown in Figure 7D, all the experimental data fall on a single linear line with a slope of 5.2. We also found that the data for DN gels of fixed network structure and λ_s but containing solvent of different viscosity also fall on the same line.[45] These results indicate that at the crack tip the yielding zone could be well approximated as uniaxial tensile deformation. The non-linear elastic fracture mechanics theory predicts the numerical constant $\gamma = 1/\pi \approx 0.32$ in Eqn. (15) for a neo-Hookean solid.[50, 51] Our experimental observation indicates a numerical constant of $\gamma = 0.19$. The slightly smaller γ of DN gels than a neo-Hookean solid is possibly related to strain hardening characteristics of the DN gels (see supplementary text in SI).

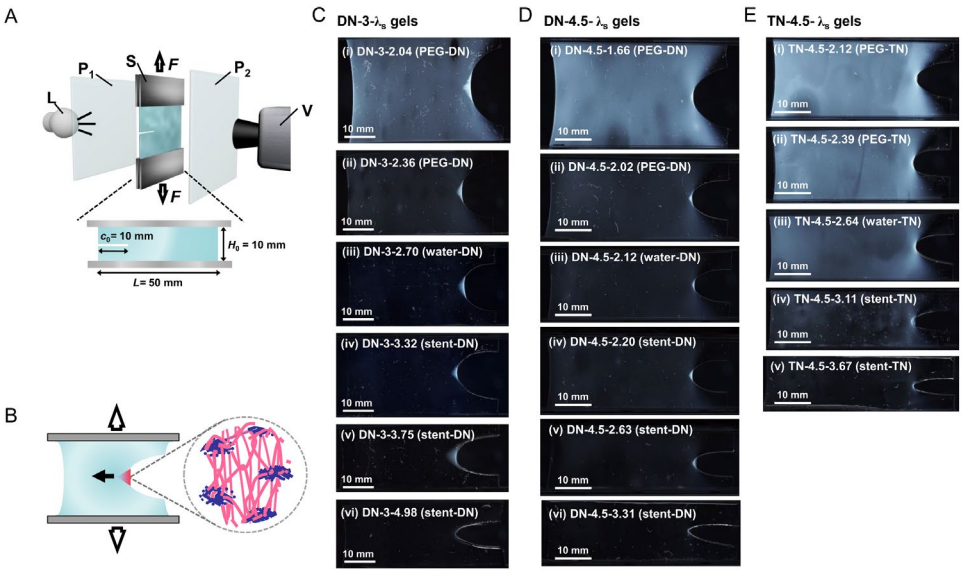

Figure 6. Birefringence observation of local yielding behaviors at the onset of crack growth for various series of DN and TN gels. (A) Schematic of real-time birefringence observation of fracture process for DN gels in pure shear test. L: lamp; P1, P2: crossed circular polarized films; S: sample; and V: video camera. Reproduced from ref [45]. Copyright (2021) National Academy of Sciences. (B) Schematic illustration of network structure in the local yielding zone ahead of the crack tip as seen by strong birefringence

area. Reproduced from ref [45]. Copyright (2021) National Academy of Sciences. (C-E) Birefringence images around the crack tip for (C) DN-3-λ_s gels, (D) DN-4.5-λ_s gels and (E) TN-4.5-λ_s gels with various λ_s.

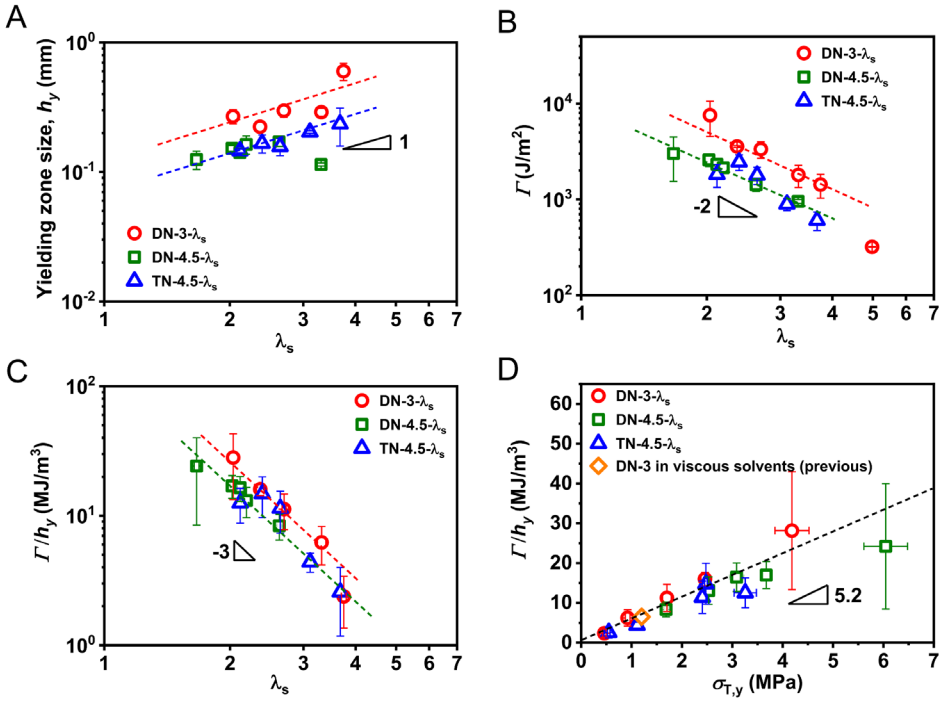

Figure 7. Effect of swelling ratio λ_s of the first network on local yielding behaviors and fracture energy at crack initiation for DN gels. (A-C) Log-log plots for yielding zone size h_y (A), fracture energy Γ (B), $\frac{\Gamma}{h_y}$ (C) as a function of λ_s for various series of DN-3-λ_s gels, DN-4.5-λ_s and TN-4.5-λ_s gels. (D) Linear plot of Γ/h_y from pure shear test and true yielding stress $\sigma_{T,y}= \sigma_y \lambda_y$ from uniaxial tensile test.

CONCLUSIONS

In summary, we have systematically studied the effect of swelling ratio of the first network on the yielding and fracture of DN and TN hydrogels with inhomogeneous first network. We find that even for DN and TN gels with inhomogeneous first network

prepared from random radical polymerization, the quantitative relations of yielding conditions of $\lambda_y \propto {\lambda_s}^{-1}$ and $\sigma_y \propto {\lambda_s}^{-2}$, independent of second network concentration, still persist. Another interesting finding is that the true yielding stress $\sigma_{T,y} = \sigma_y \lambda_y$ obeys a relation of $\sigma_{T,y} \propto {\lambda_s}^{-3}$ independent of the detailed crosslinking structure of the first network. These scaling behaviors could be well explained by a 1-D affine model of homogeneous network. On the other hand, the swelling ratio dependence of the Young's modulus suggests non-affine swelling. These results suggest that at the yielding point, the first network is largely homogenized by internal fracture prior to the yielding, and the yielding stretch ratio and yielding stress are proportional to the stretching limit and strand density of the survived first network, as like the homogeneous network. Finally, the influence of swelling λ_s on the local yielding behavior at the crack tip and the fracture toughness of the DN and TN hydrogels were investigated. We found that crack-tip yielding zone size $h_y \propto {\lambda_s}^{1}$ and fracture energy $\Gamma \propto {\lambda_s}^{-2}$. Furthermore, we found that $\frac{\Gamma}{h_y} \propto {\lambda_s}^{-3}$ is also independent of crosslinking structure and obeys a universal relationship with the true yielding stress $\lambda_y \sigma_y \propto {\lambda_s}^{-3}$ determined from the tensile tests, which is in excellent agreement with non-linear elastic fracture mechanics theory.

MATERIALS AND METHODS

Materials. 2-Acrylamido-2-methylpropanesulfonic acid sodium salt (NaAMPS; Toagosei Co., Ltd.), acrylamide (AAm; Junsei Chemical Co. Ltd.), *N*,*N*′-methylenebis(acrylamide) (MBAA; Wako Pure Chemical Industries, Ltd.), and *α*-

ketoglutaric acid (α-keto; Wako Pure Chemical Industries, Ltd.), poly(ethylene glycol) (PEG; weight-average molecular weight M_w of 20000 g/mol; Wako Pure Chemical Industries, Ltd.) were used as received. Milli-Q water (resistivity: 18.3 MΩ·cm) was used in all experiments.

Synthesis of DN and TN Hydrogels. The poly(2-acrylamido-2-methylpropanesulfonic acid sodium salt)/polyacrylamide (PNaAMPS/PAAm) DN hydrogels were synthesized by a two-step sequential network formation technique following protocol described by the literature.[34] The first network of the DN hydrogels was synthesized from an aqueous solution of 1.0 M NaAMPS containing x mol% (in this work, x = 3, 4, 4.5 or 6 mol%) crosslinking agent, MBAA, and 1 mol% initiator, α-keto. To perform the polymerization, the solution was purged in an argon atmosphere inside glove box to remove dissolved oxygen, and then transferred into a reaction cell consisting of a pair of glass plates with 0.5 mm spacing. The reaction cell was afterward irradiated with UV light (wavelength of 365 nm) for 8 h. These gels (first network) were then immersed in an aqueous solution of C_{2nd} = 2.0 M (for x= 3, 4 and 6 mol%) or 3.0 M (for x= 4.5 mol%) AAm, containing 0.01 mol% MBAA and 0.01 mol% α-keto, for one day until swelling equilibrium was reached. The polymerization was performed again by 365 nm UV irradiation for 8 h. The as-prepared DN gels were then immersed in pure water to reach equilibrium to obtain the virgin DN gels. For synthesis of the TN gels, we further repeated one more time of the swelling/polymerization process to synthesize the third network. Note that the aqueous solution used for the third network

was in the same composition with that used for the second network. The as-prepared TN gels were then immersed in pure water to reach equilibrium to obtain the virgin TN gels.

Preparation of DN and TN Hydrogels with various Swelling Ratios of the First Network. To decrease swelling ratio λ_s of the first network, the osmotic pressure method was used.[36] The virgin DN and TN gels were immersed in high osmotic pressure PEG aqueous solutions of 10 and 20 wt% to reach equilibrium. To increase λ_s, the molecular stent method was used.[13] The virgin DN and TN gels were immersed in 0.6, 1.2 and 2.5 M of NaAMPS and 0.1 mol% of α-keto aqueous solutions for at least 1 day, then polymerization of linear PNaAMPS as molecular stent was performed, after that the samples were further swelled to equilibrium in water. The sample codes, compositions, utilized methods and λ_s of the synthesized DN and TN gels are listed in Tables S1 and S2.

Tensile Test. The tensile mechanical properties of the DN and TN gels were measured with a commercial test machine (INSTRON 5965, Instron Co.) in air. The samples were cut into dumbbell shapes standardized as JISK6251-7 size (gauge length 12 mm, width 2 mm) with a gel cutting machine (Dumbbell Co., Ltd.). The nominal stress σ-stretch ratio λ curves were recorded while the sample gels were stretched at a constant velocity of 100 mm/min (strain rate of 0.14 s^{-1}). The yielding stretch ratio and yielding stress at the onset of necking, λ_y and σ_y, were determined as the nominal stretch ratio and stress at the zero-slope point of the nominal stress σ- stretch ratio λ curves, respectively. The plateau stress after yielding, $\sigma_{plateau}$, was determined as the average

stress in the plateau stress region, as illustrated in Figure S2. The stretch ratio at the onset of strain-hardening, λ_{hard}, was determined as the crossover point where the linear stress extrapolation curves in the strain-hardening region meet the plateau stress curve, as illustrated in Figure S2. The stretch ratio of the yielding zone in uniaxial tensile test λ_{yz} was roughly estimated from the stretch ratio at the onset of strain-hardening in uniaxial tensile test.

Pure-shear Fracture Test and Real-Time Birefringence Observation. The experimental setup and sample size used for real-time birefringence observation of crack propagation in DN gels during a pure shear test are illustrated in Figure 6A.[44] DN gel samples were cut using a laser cutter machine (ULTRA R5000, Universal Laser Systems, Inc.) in rectangular shapes with a length of L= 50 mm, width = 40 mm and with a pre-notch of length c_0 = 10 mm. The samples were then fixed with the pure shear clamps of a tensile tester machine (Tensilon RTC-1150A, Orientec Co.), where the initial clamp distance, H_0, was fixed at ~10 mm. The clamps were stretched by a tensile tester machine (Tensilon RTC-1150A, Orientec Co.) at a constant velocity of 50 mm/min, and the stress–stretch ratio curve was recorded. To perform real time observation, the sample is placed in between two crossed circular polarized films. One polarizing film was placed in front of a white lamp across the light path, and the other one was placed in front of the recording video camera. The fracture process was recorded in real time using an ordinary video camera (24 frames/s, 1920 × 1080 pixels, Sony α7S E-mount Camera, Sony Electronics Inc.). The entire procedure was performed in a dark room. The damage zone area S (mm^2) during the fracture process

was estimated from images of in situ recording videos using *ImageJ* Software to count the pixel numbers in the strong birefringence area ahead of the crack tip. The detailed procedure is as follows. The birefringence images were first converted to 8-bit grey images. Then, we used the highest grey value in the area far from the crack tip as the low threshold to determine the boundary of the strong birefringence area. Finally, we used the *ImageJ* software to count the pixels numbers in the strong birefringence area. To measure the fracture energy, the stress-stretch ratio curve of the un-notched sample with the same geometry as the notched sample was also measured (as shown in Figure S3). The fracture energy Γ was computed using the equation proposed by Rivlin and Thomas[52], $\Gamma = \mathrm{W}(\lambda_c) \cdot \mathrm{H}_0$. Here, $\mathrm{W}(\lambda_c) = \int_1^{\lambda_c} \sigma_{\mathrm{un-notched}}\, \mathrm{d}\lambda$ is the strain energy per unit volume (strain energy density) of the unnotched sample at λ_c, and λ_c is the critical stretch ratio at the onset of crack growth for the notched sample, as shown in Figure S3. In this research, $\mathrm{W}(\lambda_c)$ is estimated from the loading curves of the stress-stretch ratio curves. All experiments were performed at room temperature ~ 25°C.

ASSOCIATED CONTENT

Supporting Information.

Table S1. Compositions and λ_s of DN-*x*-λ_s gels.

Table S2. Compositions and λ_s of TN-*x*-λ_s gels.

Table S3. Young's modulus E_0 and the density of the elastically effective strands $\nu_{e,0}$ of the as-prepared PAMPS SN-*x* and TPEG SN.

Table S4. Theoretical stretching limit of first network strands $\lambda_{max,0}$ and elastic energy per Kuhn segment of strands $\frac{F_{el}^0}{N_x k_B T} = \frac{2E{\lambda_s}^3}{3k_B T C_0}$ for various gels.

Table S5. A list of fracture energy Γ, yielding zone area S, yielding zone deformation

ratio λ_{yz}, yielding zone size h_y, and yielding true stress $\sigma_{y,true}$ for various DN-3-λ_s gels, DN-4.5-λ_s and TN-4.5-λ_s gels.

Figure S1. Rescaled tensile behaviors in various series of DN and TN gels.

Figure S2. Determination of the parameters λ_y, σ_y, λ_{hard}, $\sigma_{plateau}$ from stress curve.

Figure S3. Typical stress curves of the notched and un-notched samples for the pure shear fracture tests.

Supplementary text on calculation of the elastic energy per Kuhn segment of strands $\frac{F_{el}^0}{N_x k_B T} = \frac{E{\lambda_s}^3}{N_x E_0} = \frac{2E{\lambda_s}^3}{3k_B T C_0}$ and the theoretical stretching limit of first network strands in relative to their as prepared reference state $\lambda_{max,0}$.

Supplementary explanation on how strain hardening characteristics affect the numerical constant γ.

AUTHOR INFORMATION

Corresponding Author

*E-mail address: gong@sci.hokudai.ac.jp (Jian Ping Gong).

Author Contributions

The manuscript was written through contributions of all authors. All authors have given approval to the final version of the manuscript.

Notes

The authors declare no competing financial interest.

ACKNOWLEDGMENT

This research is supported by the Japan Society for the Promotion of Science (JSPS) KAKENHI (grant nos. JP22H04968, JP22K21342) and by JST, PRESTO grant Number JPMJPR2098. C.Y.H. is supported by the National Science Foundation under Grant No. CMMI-1903308.

REFERENCES

(1) Rogers, J. A.; Someya, T.; Huang, Y. Materials and mechanics for stretchable electronics. *Science* **2010,** 327, 1603−1607.

(2) Martinez, R. V.; Glavan, A. C.; Keplinger, C.; Oyetibo, A. I.; Whitesides, G. M. Soft actuators and robots that are resistant to mechanical damage. *Adv. Funct. Mater.* **2014,** 24, 3003−3010.

(3) Lee, K. Y.; Mooney, D. J. Hydrogels for tissue engineering. *Chem. Rev.* **2001,** 101, 1869−1880.

(4) Minev, I. R.; Musienko, P.; Hirsch, A.; Barraud, Q.; Wenger, N.; Moraud, E. M.; Gandar, J.; Capogrosso, M.; Milekovic, T.; Asboth, L. Electronic dura mater for long-term multimodal neural interfaces. *Science* **2015,** 347, 159−163.

(5) Okumura, Y.; Ito, K. The polyrotaxane gel: A topological gel by figure-of-eight cross-links. *Adv. Mater.* **2001,** 13, 485−487.

(6) Haraguchi, K.; Takehisa, T. Nanocomposite hydrogels: A unique organic-inorganic network structure with extraordinary mechanical, optical, and swelling/de-swelling properties. *Adv. Mater.* **2002,** 14, 1120−1124.

(7) Gong, J. P.; Katsuyama, Y.; Kurokawa, T.; Osada, Y. Double-network hydrogels with extremely high mechanical strength. *Adv. Mater.* **2003,** 15, 1155−1158.

(8) Sakai, T.; Matsunaga, T.; Yamamoto, Y.; Ito, C.; Yoshida, R.; Suzuki, S.; Sasaki, N.; Shibayama, M.; Chung, U. I. Design and fabrication of a high-strength hydrogel with ideally homogeneous network structure from tetrahedron-like macromonomers. *Macromolecules* **2008,** 41, 5379−5384.

(9) Gong, J. P. Why are double network hydrogels so tough? *Soft Matter* **2010,** 6, 2583−2590.

(10) Sun, J. Y.; Zhao, X. H.; Illeperuma, W. R. K.; Chaudhuri, O.; Oh, K. H.; Mooney, D. J.; Vlassak, J. J.; Suo, Z. G. Highly stretchable and tough hydrogels. *Nature* **2012,** 489, 133−136.

(11) Sun, T. L.; Kurokawa, T.; Kuroda, S.; Ihsan, A. B.; Akasaki, T.; Sato, K.; Haque,

M. A.; Nakajima, T.; Gong, J. P. Physical hydrogels composed of polyampholytes demonstrate high toughness and viscoelasticity. *Nat. Mater.* **2013,** 12, 932−937.

(12) Ducrot, E.; Chen, Y.; Bulters, M.; Sijbesma, R. P.; Creton, C. Toughening elastomers with sacrificial bonds and watching them break. *Science* **2014,** 344, 186−189.

(13) Nakajima, T.; Sato, H.; Zhao, Y.; Kawahara, S.; Kurokawa, T.; Sugahara, K.; Gong, J. P. A universal molecular stent method to toughen any hydrogels based on double network concept. *Adv. Funct. Mater.* **2012,** 22, 4426−4432.

(14) Matsuda, T.; Nakajima, T.; Gong, J. P. Fabrication of tough and stretchable hybrid double-network elastomers using ionic dissociation of polyelectrolyte in nonaqueous media. *Chem. Mater.* **2019,** 31, 3766−3776.

(15) Zheng, Y.; Kiyama, R.; Matsuda, T.; Cui, K.; Li, X.; Cui, W.; Guo, Y.; Nakajima, T.; Kurokawa, T.; Gong, J. P. Nanophase separation in immiscible double network elastomers induces synergetic strengthening, toughening, and fatigue resistance. *Chem. Mater.* **2021,** 33, 3321−3334.

(16) Nakajima, T.; Ozaki, Y.; Namba, R.; Ota, K.; Maida, Y.; Matsuda, T.; Kurokawa, T.; Gong, J. P. Tough Double-Network Gels and Elastomers from the Nonprestretched First Network. *ACS Macro Lett.* **2019,** 8, 1407−1412.

(17) Nakajima, T. Generalization of the sacrificial bond principle for gel and elastomer toughening. *Polym. J.* **2017,** 49, 477−485.

(18) Na, Y.-H.; Tanaka, Y.; Kawauchi, Y.; Furukawa, H.; Sumiyoshi, T.; Gong, J. P.; Osada, Y. Necking phenomenon of double-network gels. *Macromolecules* **2006,** 39, 4641−4645.

(19) Webber, R. E.; Creton, C.; Brown, H. R.; Gong, J. P. Large strain hysteresis and mullins effect of tough double-network hydrogels. *Macromolecules* **2007,** 40, 2919−2927.

(20) Nakajima, T.; Kurokawa, T.; Ahmed, S.; Wu, W.-l.; Gong, J. P. Characterization of internal fracture process of double network hydrogels under uniaxial elongation. *Soft Matter* **2013,** 9, 1955−1966.

(21) Matsuda, T.; Nakajima, T.; Fukuda, Y.; Hong, W.; Sakai, T.; Kurokawa, T.; Chung, U.-i.; Gong, J. P. Yielding criteria of double network hydrogels. *Macromolecules* **2016,** 49, 1865−1872.

(22) Guo, H.; Hong, W.; Kurokawa, T.; Matsuda, T.; Wu, Z. L.; Nakajima, T.; Takahata, M.; Sun, T.; Rao, P.; Gong, J. P. Internal damage evolution in double-network hydrogels studied by microelectrode technique. *Macromolecules* **2019,** 52, 7114−7122.

(23) Kiyama, R.; Yoshida, M.; Nonoyama, T.; Sedlačík, T.; Jinnai, H.; Kurokawa, T.; Nakajima, T.; Gong, J. P. Nanoscale TEM Imaging of Hydrogel Network Architecture. *Adv. Mater.* **2022**, 2208902.

(24) Seiffert, S. Origin of nanostructural inhomogeneity in polymer-network gels. *Polym. Chem.* **2017,** 8, 4472−4487.

(25) Ide, N.; Fukuda, T. Nitroxide-controlled free-radical copolymerization of vinyl and divinyl monomers. 2. Gelation. *Macromolecules* **1999,** 32, 95−99.

(26) Seiffert, S. Scattering perspectives on nanostructural inhomogeneity in polymer network gels. *Prog. Polym. Sci.* **2017,** 66, 1−21.

(27) Kizilay, M. Y.; Okay, O. Effect of hydrolysis on spatial inhomogeneity in poly (acrylamide) gels of various crosslink densities. *Polymer* **2003,** 44, 5239−5250.

(28) Kizilay, M. Y.; Okay, O. Effect of initial monomer concentration on spatial inhomogeneity in poly (acrylamide) gels. *Macromolecules* **2003,** 36, 6856−6862.

(29) Tsukeshiba, H.; Huang, M.; Na, Y. H.; Kurokawa, T.; Kuwabara, R.; Tanaka, Y.; Furukawa, H.; Osada, Y.; Gong, J. P. Effect of polymer entanglement on the toughening of double network hydrogels. *J. Phys. Chem. B* **2005,** 109, 16304−16309.

(30) Orakdogen, N.; Okay, O. Correlation between crosslinking efficiency and spatial inhomogeneity in poly (acrylamide) hydrogels. *Polym. Bull.* **2006,** 57, 631−641.

(31) Orakdogen, N.; Okay, O. Influence of the initiator system on the spatial inhomogeneity in acrylamide-based hydrogels. *J. Appl. Polym. Sci.* **2007,** 103, 3228−3237.

(32) Norisuye, T.; Tran-Cong-Miyata, Q.; Shibayama, M. Dynamic inhomogeneities in polymer gels investigated by dynamic light scattering. *Macromolecules* **2004,** 37,

2944−2953.

(33) Shibayama, M.; Shirotani, Y.; Shiwa, Y. Static inhomogeneities and dynamics of swollen and reactor-batch polymer gels. *J. Chem. Phys.* **2000,** 112, 442−449.

(34) Bastide, J.; Leibler, L. Large-scale heterogeneities in randomly cross-linked networks. *Macromolecules* **1988,** 21, 2647−2649.

(35) Shibayama, M. Spatial inhomogeneity and dynamic fluctuations of polymer gels. *Macromol. Chem. Phys.* **1998,** 199, 1−30.

(36) Ahmed, S.; Nakajima, T.; Kurokawa, T.; Haque, M. A.; Gong, J. P. Brittle–ductile transition of double network hydrogels: Mechanical balance of two networks as the key factor. *Polymer* **2014,** 55, 914−923.

(37) Sedlačík, T. s.; Nonoyama, T.; Guo, H.; Kiyama, R.; Nakajima, T.; Takeda, Y.; Kurokawa, T.; Gong, J. P. Preparation of tough double-and triple-network supermacroporous hydrogels through repeated cryogelation. *Chem. Mater.* **2020,** 32, 8576−8586.

(38) Cui, K.; Ye, Y. N.; Sun, T. L.; Chen, L.; Li, X.; Kurokawa, T.; Nakajima, T.; Nonoyama, T.; Gong, J. P. Effect of structure heterogeneity on mechanical performance of physical polyampholytes hydrogels. *Macromolecules* **2019,** 52, 7369−7378.

(39) Zhang, Y.; Fukao, K.; Matsuda, T.; Nakajima, T.; Tsunoda, K.; Kurokawa, T.; Gong, J. P. Unique crack propagation of double network hydrogels under high stretch. *Extreme Mech. Lett.* **2021**, 101588.

(40) Fukao, K.; Tanaka, K.; Kiyama, R.; Nonoyama, T.; Gong, J. P. Hydrogels toughened by biominerals providing energy-dissipative sacrificial bonds. *J. Mater. Chem. B* **2020,** 8, 5184−5188.

(41) Wang, S.; Panyukov, S.; Craig, S. L.; Rubinstein, M. Contribution of Unbroken Strands to the Fracture of Polymer Networks. *Macromolecules* **2023,** 56, 2309–2318.

(42) Rubinstein, M.; Colby, R. H., *Polymer physics*. Oxford university press New York: 2003; Vol. 23; pg. 180.

(43) Hoshino, K.-i.; Nakajima, T.; Matsuda, T.; Sakai, T.; Gong, J. P. Network elasticity of a model hydrogel as a function of swelling ratio: from shrinking to extreme swelling

states. *Soft Matter* **2018,** 14, 9693−9701.

(44) Panyukov, S. Scaling theory of high elasticity. *Sov. Phys. JETP* **1990,** 71, 372-379.

(45) Zheng, Y.; Matsuda, T.; Nakajima, T.; Cui, W.; Zhang, Y.; Hui, C.-Y.; Kurokawa, T.; Gong, J. P. How chain dynamics affects crack initiation in double-network gels. *Proc. Natl. Acad. Sci. U.S.A.* **2021,** 118, e2111880118.

(46) Matsuda, T.; Kawakami, R.; Nakajima, T.; Hane, Y.; Gong, J. P. Revisiting the Origins of the Fracture Energy of Tough Double-Network Hydrogels with Quantitative Mechanochemical Characterization of the Damage Zone. *Macromolecules* **2021,** 54, 10331−10339.

(47) Matsuda, T.; Kawakami, R.; Nakajima, T.; Gong, J. P. Crack tip field of a double-network gel: Visualization of covalent bond scission through mechanoradical polymerization. *Macromolecules* **2020,** 53, 8787−8795.

(48) Yu, Q. M.; Tanaka, Y.; Furukawa, H.; Kurokawa, T.; Gong, J. P. Direct observation of damage zone around crack tips in double-network gels. *Macromolecules* **2009,** 42, 3852−3855.

(49) Slootman, J.; Yeh, C. J.; Millereau, P.; Comtet, J.; Creton, C. A molecular interpretation of the toughness of multiple network elastomers at high temperature. *Proc. Natl. Acad. Sci. U.S.A.* **2022,** 119, e2116127119.

(50) Long, R.; Hui, C.-Y.; Gong, J. P.; Bouchbinder, E. The Fracture of Highly Deformable Soft Materials: A Tale of Two Length Scales. *Annu. Rev. Condens. Matter Phys.* **2021,** 12, 71−94.

(51) Long, R.; Hui, C.-Y. Crack tip fields in soft elastic solids subjected to large quasi-static deformation—a review. *Extreme Mech. Lett.* **2015,** 4, 131−155.

(52) Rivlin, R.; Thomas, A. G. Rupture of rubber. I. Characteristic energy for tearing. *J. Polym. Sci.* **1953,** 10, 291−318.